

# BIPOLAR CONDUCTION and DRAIN-INDUCED BARRIER THINNING in CARBON NANOTUBE FETs

J.P. Clifford, D.L. John, *Student Member, IEEE*, and D.L. Pulfrey, *Fellow, IEEE*

Department of Electrical and Computer Engineering  
University of British Columbia  
Vancouver, BC V6T 1Z4, Canada  
*contact:* pulfrey@ece.ubc.ca or jasonc@ece.ubc.ca

## ABSTRACT

The drain current-voltage ( $I$ - $V$ ) characteristics of Schottky-barrier carbon nanotube FETs are computed via a self-consistent solution to the 2-D potential profile, the electron and hole charges in the nanotube, and the electron and hole currents. These out-of-equilibrium results are obtained by allowing splitting of both the electron and hole quasi-Fermi levels to occur at the source and drain contacts to the tube, respectively. The interesting phenomena of bipolar conduction in a FET, and of drain-induced barrier thinning (DIBT) are observed. These phenomena are shown to add a breakdown-like feature to the drain  $I$ - $V$  characteristic. It is also shown that a more traditional, saturating-type characteristic can be obtained by workfunction engineering of the source and drain contacts.

## 1 INTRODUCTION

In Schottky-barrier carbon nanotube field-effect transistors (SB-CNFETs), the gate electrode spans the entire length of an intrinsic nanotube, and transistor action is achieved by the modulation, by the gate, of the Schottky-barrier profiles at the interfaces to the tube at the source and drain contacts [1, 2]. At equilibrium, when the distribution functions of the carriers in the tube are known, it is relatively straight-forward to obtain a self-consistent solution to the charge and potential profiles [3]. Out-of-equilibrium, the situation is complicated by the fact that the hot carriers injected into the tube by tunneling and thermionic emission at the contacts are likely to travel quasi-ballistically. The situation is not unlike that in extremely short-basewidth HBTs, in which the reduced opportunities for scattering lead to electron distribution functions that are highly distorted from their equilibrium forms [4]. Nevertheless, it has been common practice in modeling HBTs to employ quasi-equilibrium statistics via a splitting of the minority-carrier quasi-Fermi level (QFL) at the hetero-interface between the emitter and the highly doped base [5, 6, 7]. It is possible with this approach to get good agreement in the DC characteristics with results from a complete solution to the Boltzmann Transport Equation [8].

In this work, we apply the principle of QFL-splitting to SB-CNFETs. Because the simultaneous injection of electrons and holes is possible [3, 9], and the nanotubes considered here are intrinsic, it is necessary to account for the splitting of both the electron and hole QFLs. This allows both the electron and hole currents to be computed in a manner that is

entirely self-consistent with the non-equilibrium charge on the nanotube and the potential profile within the transistor. Thus, it is possible to obtain a more rigorous self-consistent solution than has been achieved hitherto [10, 11]. This new modeling feature not only clearly reveals the transition from unipolar to bipolar conduction in SB-CNFETs, but it also predicts the occurrence of a new phenomenon, namely: drain-induced barrier thinning (DIBT). In the latter condition, the source/tube barrier is modulated by the drain-source voltage, leading to increased electron current at high source-drain biases. These bipolar phenomena occur at a single polarity of gate bias and, therefore, are to be distinguished from the previously reported ambipolar property of SB-CNFETS [12], which referred to the ability of these devices to be either mainly electron-conducting, or mainly hole-conducting, depending on the polarity of the gate bias. We show that a more traditional, unipolar, saturating-type, drain  $I$ - $V$  characteristic can be obtained if bipolar effects are suppressed by choosing metals of appropriate workfunction for the source and drain contacts.

## 2 METHODOLOGY

For a SB-CNFET, the general, non-equilibrium situation, *i.e.*, when  $V_{DS} \neq 0$ , is illustrated in Fig. 1. This figure identifies the electron and hole QFLs, and also indicates how the split in the electron QFL,  $\Delta E_{Fn}$ , is referenced to the source Fermi energy, and how the split in the hole QFL,  $\Delta E_{Fp}$ , is referenced to the drain Fermi energy. Fig. 1 also shows the various electron and hole fluxes at the two ends of the nanotube. Considering the electron fluxes at the source/tube interface, for example,  $F_1$  is a flux of electrons originating from the source, and  $F_2$  is a flux of electrons flowing into the source from the tube. The latter arises from reflection at the tube/drain potential barrier, and injection from the drain. Backscattering within the tube would also contribute to  $F_2$ , but is not considered here as we are assuming ballistic transport. This assumption allows the QFLs to be kept constant along the length of the tube. If scattering were significant, there would be a gradient in the QFLs, commensurate with a drift/diffusion current, which would serve to reduce the drain current from the values predicted in this paper.

The energy point of reference is taken to be the source, at which the Fermi-Dirac distribution function is  $f(E)$ , where  $E$  is the energy. The charge in flux  $F_2$  is characterized by a QFL,  $E_{Fn}$ , which differs from the equilibrium Fermi-level at the source, giving rise to a quasi-Fermi-Dirac distribution  $f(E - E_{Fn})$ . Both fluxes  $F_1$  and  $F_2$  traverse the source/tube potential barrier by tunneling and thermionic emission, and can be described in the Landauer formalism [13]:

$$F_1 = \frac{2}{\pi\hbar} \int_{E_C}^{\infty} T_{Sn}(E) f(E) dE \quad (1)$$

$$F_2 = \frac{2}{\pi\hbar} \int_{E_C}^{\infty} T_{Sn}(E) f(E - E_{Fn}) dE, \quad (2)$$

where  $T_{Sn}$  is the transmission probability for electrons at the source barrier, and  $E_C$  is the energy of the essentially flat conduction band edge in the region of the tube distal from the contacts. The factor of 2 that arises in each of the above equations is a result of double degeneracy in the lowest subband. Only the lowest energy subbands are included since the

contribution of all higher subbands is negligible. The corresponding expressions for the electron fluxes at the drain end of the tube are:

$$F_3 = \frac{2}{\pi\hbar} \int_{E_C}^{\infty} T_{Dn}(E) f(E - E_{Fn}) dE \quad (3)$$

$$F_4 = \frac{2}{\pi\hbar} \int_{E_C}^{\infty} T_{Dn}(E) f(E + qV_{DS}) dE, \quad (4)$$

where  $T_{Dn}$  is the transmission probability for electrons at the drain barrier,  $q$  is the magnitude of the electronic charge and  $V_{DS}$  is the applied drain-source bias. Continuity of electron current, in the absence of recombination in the tube and leakage to the gate, implies

$$F_1 - F_2 = F_3 - F_4. \quad (5)$$

The corresponding expression for holes, with reference to Fig. 1, is

$$F_6 - F_5 = F_8 - F_7, \quad (6)$$

where the sign conventions for the two flux-balance equations have been chosen to give a positive drain current. The individual components of the hole fluxes can be defined similarly to the electron fluxes, using a hole QFL,  $E_{Fp}$ , and hole transmission probabilities at the source and drain,  $T_{Sp}$  and  $T_{Dp}$ , respectively. Rearranging (5) and (6), two equations, suitable for minimization by Newton's method with  $E_{Fn}$  and  $E_{Fp}$  as independent variables, can be formulated:

$$\int_{E_C}^{\infty} [T_{Sn}(E) f(E) + T_{Dn}(E) f(E + qV_{DS}) - (T_{Sn}(E) + T_{Dn}(E)) f(E - E_{Fn})] dE = 0 \quad (7)$$

and

$$\int_{-\infty}^{E_V} [T_{Sp}(E) f(E) + T_{Dp}(E) f(E - qV_{DS}) - (T_{Sp}(E) + T_{Dp}(E)) f(E + E_{Fp})] dE = 0, \quad (8)$$

where  $E_V$  is the energy of the essentially flat valence band edge in the region of the tube distal from the contacts. The transmission probabilities are computed using the WKB approximation, with a value of unity being assumed in the case of thermionic emission.

The self-consistent solution procedure begins by assuming values for the QFLs,  $E_{Fn}$  and  $E_{Fp}$ , and then using these to compute the electron and hole charges that are used in a numerical, finite-element, two-dimensional solution of Poisson's equation [3]. From the potential profile the tunneling probabilities are then computed, and used to determine the various fluxes. The flux-balance equations, (5) and (6), are then solved to yield new values for  $E_{fn}$  and  $E_{fp}$ . Iterations of the entire procedure are performed until the differences between the starting and calculated QFLs are within the prescribed tolerance. Note that, while the flux calculations assume independent electron and hole fluxes, the self-consistent solution for potential and charge takes both fluxes into account, so that the final barrier profiles depend on the concentrations of both electrons and holes.

The total current,  $I$ , and the electron and hole currents,  $I_n$  and  $I_p$ , respectively, are given by

$$I = I_n + I_p, \quad (9)$$

where, for example,

$$I_n = q(F_1 - F_2) \quad (10)$$

$$I_p = q(F_6 - F_5). \quad (11)$$

### 3 RESULTS AND DISCUSSION

Results are presented for (16,0) tubes having a radius of 0.63 nm and a length of 100 nm. The tube “wall” is taken to be infinitesimally thin, and the permittivity of the interior space is assumed to be  $\epsilon_0$ , the free-space value. The coaxial structure considered is shown in Fig. 2 [3, 11]; the gate radius is 6.3 nm and the gate-insulator permittivity is  $3.9\epsilon_0$ . The bandgap of the carbon nanotube is 0.63 eV, and the work functions of the tube,  $\Phi_{CN}$ , and of the gate-, source-, and drain-metallizations,  $\Phi_G$ ,  $\Phi_S$ , and  $\Phi_D$ , respectively, are taken to be 4.5 eV, unless otherwise stated. This specification implies that there is no band-bending when there is no applied bias. Further, because of the use of an intrinsic nanotube, the Fermi levels of the source and drain metals lie in the middle of the nanotube’s bandgap. The temperature is taken to be 300K. It is known that SB-CNFETs are ambipolar, meaning that both  $n$ -type and  $p$ -type conduction is possible, depending on the polarity of the gate-source bias,  $V_{GS}$  [12]. Here we confine the treatment to  $V_{GS} > 0$ , and report on new bipolar conduction phenomena.

A typical evolution of the energy band diagram for the device is depicted in Fig. 3, which considers the case of  $V_{GS} = 0.3$  V. As  $V_{DS}$  is increased from 0 to 0.3 V, the potential “spike” at the drain end of the tube is progressively diminished. The two consequences of this are: (i) flux  $F_3$  is increased due to the reduced barrier height; (ii) flux  $F_4$  is decreased due to the reduced transparency of the barrier for electrons tunneling from the drain. Thus, under these conditions, the drain current is almost entirely electronic, as can be seen from Fig. 4. In the absence of recombination, the net flux,  $(F_3 - F_4)$ , must also be manifest at the source/tube interface. Initially, this is accomplished by a reduction in  $F_2$ , *i.e.*, a split,  $\Delta E_{Fn}$ , appears in the electron QFL. There is also a slight splitting,  $\Delta E_{Fp}$ , of the hole QFL, to accommodate the small, net hole flux,  $(F_8 - F_7)$ , that arises because of the reduction in the barrier presented to hole thermionic emission from the drain into the tube.

When  $V_{DS} > V_{GS}$ , a “spike” appears in the valence band edge at the drain end of the tube, facilitating the flow of holes into the nanotube, *i.e.*  $F_8 > F_7$ , and causing  $\Delta E_{Fp}$  to increase (see Fig. 5). The concomitant increase in hole charge drives the nanotube towards charge neutrality in the mid-length region between the potential barriers. Thus, the gate potential starts to couple more effectively to the source and drain, resulting in a thinning of the two potential barriers. The effect is shown clearly in Fig. 3(d), and results in a dramatic increase in *both* hole *and* electron currents (see Fig. 4). Thus, under these bias conditions the SB-CNFET exhibits distinctive bipolar behaviour. We suggest that the label of Drain-Induced-Barrier-Thinning (DIBT) be given to the phenomenon responsible for the sudden increase of electron current.

In practice, the extent to which DIBT allows  $I_n$  to remain the dominant contributor to  $I_D$  will depend on the ratio of  $V_{DS}$  to  $V_{GS}$ . This is because the hole current,  $I_p$ , increases due to the direct effect of  $V_{DS}$  on the thinning of the tunneling barrier at the drain. From Fig. 3 it can be appreciated that for larger  $V_{GS}$ , a larger  $V_{DS}$  is required to invert the slope of the band-bending

at the drain, thereby facilitating the flow of holes. Our simulations show, generally, that the “cross-over” point from mainly electron conduction to mainly hole conduction occurs at  $V_{DS} = 2V_{GS}$ . Fig. 4 shows a particular example of this, for the case of  $V_{GS} = 0.3$  V. Associated with these electron and hole currents will be the simultaneous presence of large electron and hole concentrations, which might lead to significant recombination. Although this phenomenon is not yet incorporated in our model, we can anticipate that maximum recombination will occur, *for a fixed*  $V_{DS}$ , when the product  $(I_n I_p)$  is a maximum. Our simulations reveal that this condition is reached when  $V_{GS} = V_{DS}/2$ , which is precisely the bias conditions under which maximum radiative recombination has been observed experimentally from planar SB-CNFETs, yielding the smallest electrically controlled light source yet reported [9]. Further confirmation of the relevance of the present model to device analysis comes from the family of drain  $I$ - $V$  curves shown in Figs. 6(a) and (b). These characteristics are very similar to those which have been obtained experimentally by others, *e.g.*, in Fig. 1(c) of Ref. [9].

The bipolar phenomena described above are interesting new features of SB-CNFETs that give the drain  $I$ - $V$  characteristic a breakdown-like appearance. However, more traditional FET behaviour, in the form of a “linear-triode-saturation” characteristic, is also possible. For the workfunctions considered thus far, such a characteristic could occur at low  $V_{DS}$  and, as Fig. 4 indicates, would result in very low saturation currents. One way of obtaining higher saturation currents, and to have them persist to larger  $V_{DS}$ , would be to change the workfunctions of the source- and/or drain-metallizations. An example of this “workfunction engineering” concept is shown in Fig. 7. The bottom curve on this figure is for the device we have been considering thus far, *i.e.*,  $\Phi_S = \Phi_D = \Phi_{CN} = 4.5$  eV. By reducing  $\Phi_D$  to 4.3 eV, there is noticeable current saturation before the onset of breakdown. This is primarily due to the diminishing of the barrier to electrons on the nanotube side of the drain (refer to Fig. 3(a)), which allows  $F_3$  to increase. The counter-directed flow,  $F_4$ , is affected in two compensatory ways, namely: it would decrease due to a reduction in the barrier transparency to tunneling, yet increase due to a reduction in barrier height. If,  $\Phi_S$  is reduced, instead of  $\Phi_D$ , the electron flux  $F_1$  issuing from the source is increased, but the net flux at the drain is constrained by the barrier existing at the tube/drain interface. Saturation of  $I_D$  does not occur until this barrier is removed by the applied  $V_{DS}$ . A reduction in the saturation voltage,  $V_{DS,sat}$ , and a prolongation of the saturation current,  $I_{D,sat}$ , can be achieved by reducing both  $\Phi_S$  and  $\Phi_D$ , as demonstrated by the top curve in Fig. 7. These results indicate that the workfunctions of the source and drain contacts determine whether a SB-CNFET exhibits either a “saturating” or a “continuously increasing” characteristic. Experimentally, characteristics of the former type [2], and of the latter type [9], have both been observed, and it could be that differences in contact workfunction are responsible for this range of behaviour.

## 4 CONCLUSIONS

From this theoretical study of coaxial, Schottky-barrier carbon nanotube FETs operating under quasi-equilibrium conditions, it can be concluded that:

1. contrarily to the behaviour in other field-effect devices, the presence of Schottky barriers at the source and drain leads to the possibility of the drain current having a bipolar

character;

2. this bipolar conduction is accentuated by a new phenomenon, drain-induced barrier thinning, DIBT, in which the tunneling of electrons from the source into the nanotube is enhanced by source/nanotube barrier modification due to  $V_{DS}$ ;
3. when bipolar conduction occurs, it occasions a large rise in the drain current, as is usually associated with breakdown;
4. the simultaneous presence of large concentrations of electrons and holes in the nanotube indicates that significant recombination may occur. The bias conditions under which this might happen have been shown here to be those under which radiative recombination has been observed experimentally;
5. more traditional, unipolar conduction, leading to the usual, saturation-type drain  $I$ - $V$  characteristics can be obtained by workfunction engineering of the source and drain contacts.

## **Acknowledgements**

The authors gratefully acknowledge: L.C. Castro, P.J.S. Pereira, and D. Ong for stimulating conversations; R. Martel for making available Ref. [9] prior to its publication; and NSERC for financial support.

## References

- [1] S. Heinze, J. Tersoff, R. Martel, V. Derycke, J. Appenzeller, and Ph. Avouris, “Carbon nanotubes as Schottky barrier transistors,” *Phys. Rev. Lett.*, vol. 89, no. 10, pp. 106801-1–106801-4, 2002.
- [2] J. Appenzeller, J. Knoch, V. Derycke, R. Martel, S. Wind, and Ph. Avouris, “Field-modulated carrier transport in carbon nanotube transistors,” *Phys. Rev. Lett.*, vol. 89, no. 12, pp. 126801-1–126801-4, 2002.
- [3] D.L. John, L.C. Castro, J.P. Clifford, and D.L. Pulfrey, “Electrostatics of coaxial Schottky-barrier nanotube field-effect transistors,” *IEEE Trans. Nanotechnol.*, accepted for publication, May 21, 2003.
- [4] A.R. St.Denis and D.L. Pulfrey, “Quasiballistic transport in GaAs-based heterojunction and homojunction bipolar transistors,” *J. Appl. Phys.*, vol. 84, no. 9, pp. 4959–4965, 1998.
- [5] A.A. Grinberg, M.S. Shur, R.J. Fischer, and H. Morkoç, “An investigation of the effect of graded-layers and tunneling on the performance of AlGaAs/GaAs heterojunction bipolar transistors,” *IEEE Trans. Electron Devices*, vol. ED-31, pp. 1758–1765, 1984.
- [6] M.S. Lundstrom, “Boundary conditions for  $pn$  heterojunctions,” *Solid-State Electron.*, vol. 27, pp. 491–496, 1984.
- [7] D.L. Pulfrey and S. Searles, “Electron quasi-Fermi level splitting at the base-emitter junction of AlGaAs/GaAs HBT’s,” *IEEE Trans. Electron Devices*, vol. 40, no. 6, pp. 1183-1185, 1993.
- [8] D.L. Pulfrey, “Modeling high-performance HBTs,” in *High-speed Heterostructure Devices*, P Roblin and H. Rohdin, Eds., New York: Cambridge University Press, 2002, ch. 18.
- [9] J.A. Misewich, R. Martel, Ph. Avouris, J.C. Tsang, S. Heinze and J. Tersoff, “Electrically induced optical emission from a carbon nanotube FET,” *Science*, vol. 300, pp. 783–786, 2003.
- [10] J. Guo, M. Lundstrom, and S. Datta, “Performance projections for ballistic carbon nanotube field-effect transistors,” *Appl. Phys. Lett.*, vol. 80, no. 17, pp. 3192–3194, 2002.
- [11] L.C. Castro, D.L. John, and D.L. Pulfrey, “Towards a compact model for Schottky-barrier nanotube FETs,” in *Proc. IEEE COMMAD*, Dec. 11–13, 2002, accepted for publication, Apr. 7, 2003.
- [12] R. Martel, V. Derycke, C. Lavoie, J. Appenzeller, K.K. Chan, J. Tersoff, and Ph. Avouris, “Ambipolar electrical transport in semiconducting single-wall carbon nanotubes,” *Phys. Rev. Lett.*, vol. 87, no. 25, pp. 256805-1–256805-4, 2001.
- [13] D.K. Ferry and S.M. Goodnick, *Transport in Nanostructures*, pp. 124–131, New York: Cambridge University Press, 1997.

# List of Figures

1	Energy band diagram under non-equilibrium conditions, showing: the electron and hole quasi-Fermi levels, $E_{Fn}$ (dashed line) and $E_{Fp}$ (stippled line), respectively; the splitting of the two QFLs; and the various electron and hole fluxes, $F_1$ to $F_4$ , and $F_5$ to $F_8$ , respectively. . . . .	9
2	SB-CNFET model geometry. The gate forms the curved surface of the outer cylinder, and the source and drain form the two ends. The semiconducting nanotube is placed coaxially with the outer cylinder. . . . .	10
3	Energy band diagrams showing the positions of the QFLs, $E_{Fn}$ (dashed line) and $E_{Fp}$ (stippled line), for $V_{GS} = 0.3$ V at various values of $V_{DS}$ . . . . .	11
4	Drain $I$ - $V$ characteristic at $V_{GS} = 0.3$ V, showing the contributions from both electrons (dashed line) and holes (stippled line) to the total drain current. . . . .	12
5	Dependence of QFL splits $\Delta E_{Fn}$ and $\Delta E_{Fp}$ on bias for: (1) $V_{GS} = 0.0$ V, (2) $V_{GS} = 0.1$ V, (3) $V_{GS} = 0.3$ V, and (4) $V_{GS} = 0.5$ V. Note that $\Delta E_{Fn} = E_{Fn}$ and $\Delta E_{Fp} = E_{Fp} + qV_{DS}$ , as shown in Figure 1, and $E_{Fn}$ and $E_{Fp}$ are negative values. . . . .	13
6	Drain $I$ - $V$ characteristics: (a) linear plot, (b) log-linear plot. . . . .	14
7	Drain $I$ - $V$ characteristics for different workfunctions at the contacts to the nanotube at $V_{GS} = 0.5$ V. . . . .	15

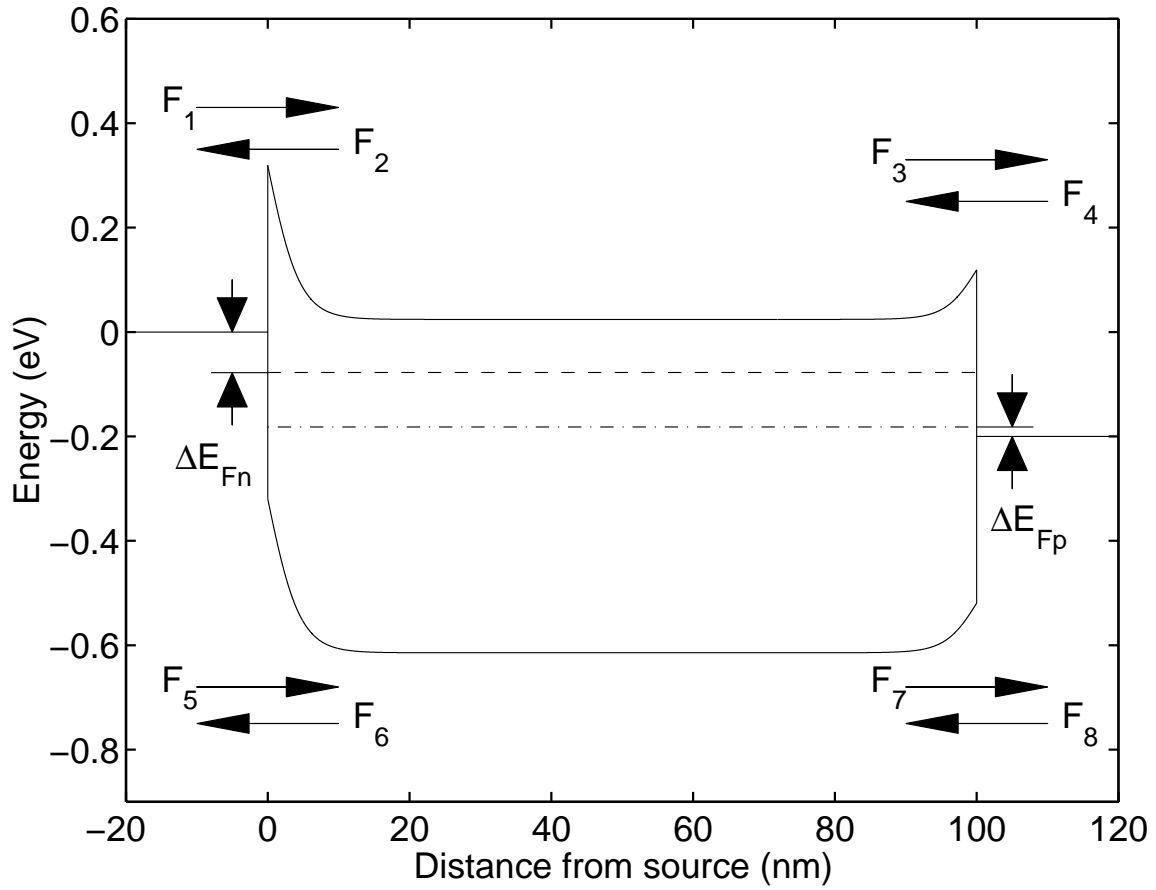


Figure 1: Energy band diagram under non-equilibrium conditions, showing: the electron and hole quasi-Fermi levels,  $E_{Fn}$  (dashed line) and  $E_{Fp}$  (stippled line), respectively; the splitting of the two QFLs; and the various electron and hole fluxes,  $F_1$  to  $F_4$ , and  $F_5$  to  $F_8$ , respectively.

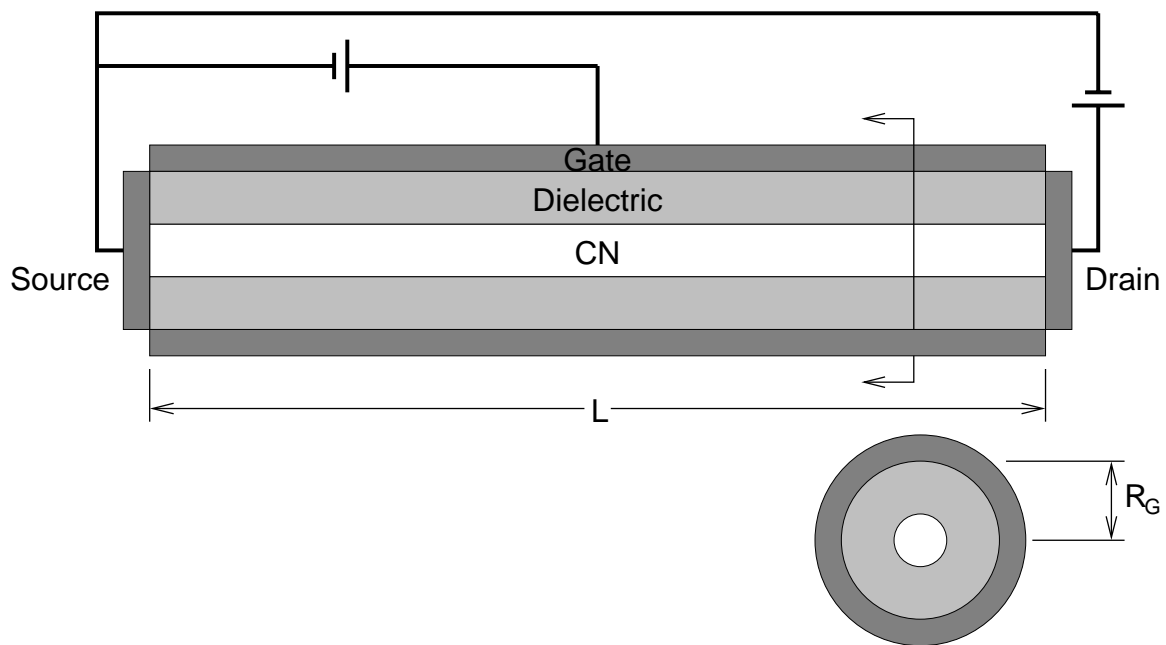


Figure 2: SB-CNFET model geometry. The gate forms the curved surface of the outer cylinder, and the source and drain form the two ends. The semiconducting nanotube is placed coaxially with the outer cylinder.

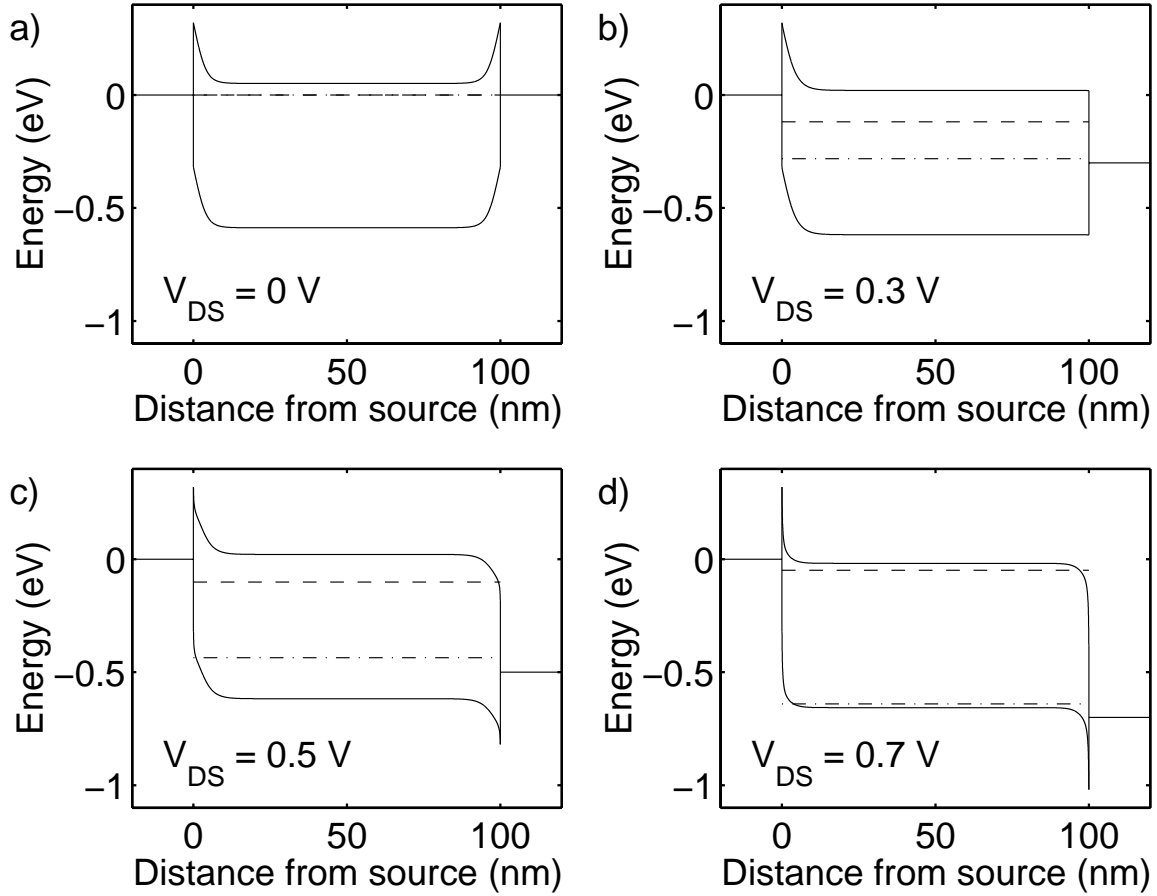


Figure 3: Energy band diagrams showing the positions of the QFLs,  $E_{Fn}$  (dashed line) and  $E_{Fp}$  (stippled line), for  $V_{GS} = 0.3$  V at various values of  $V_{DS}$ .

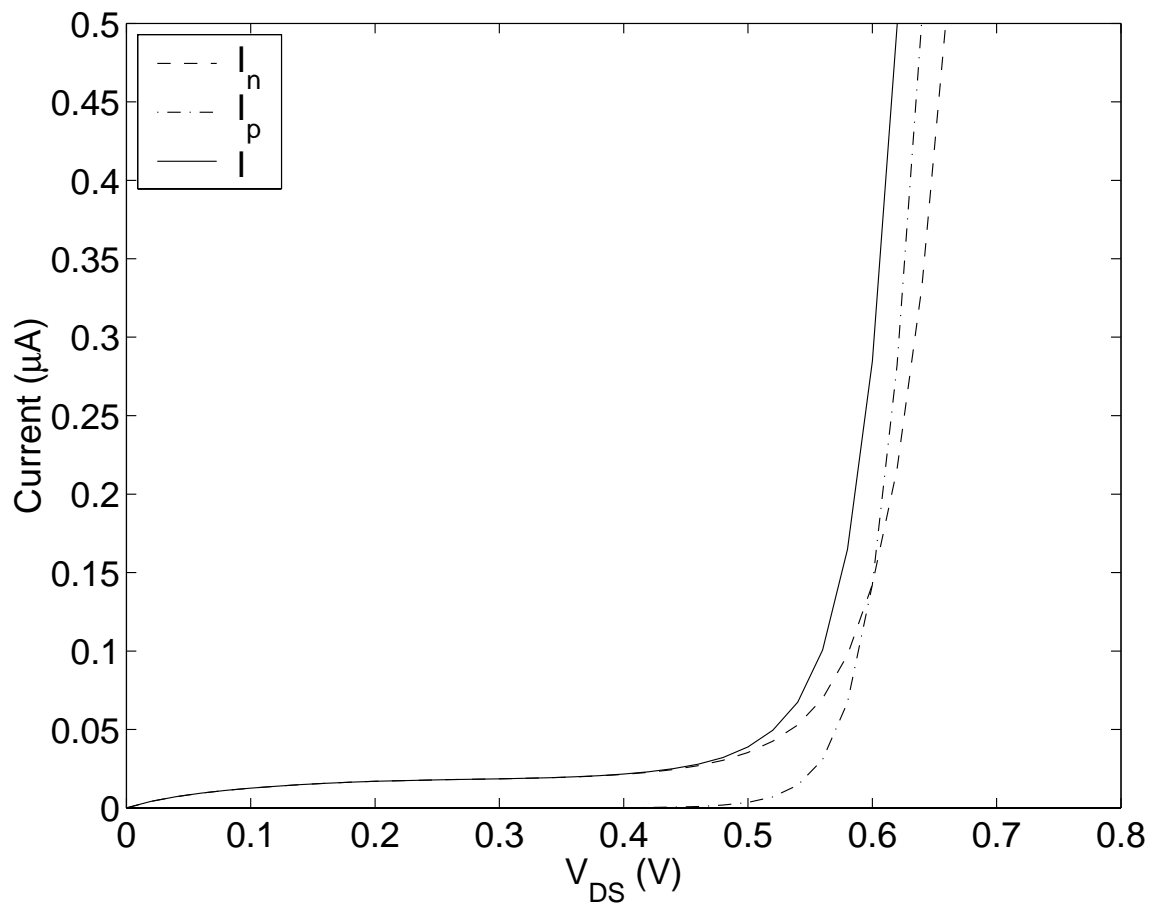


Figure 4: Drain  $I$ - $V$  characteristic at  $V_{GS} = 0.3$  V, showing the contributions from both electrons (dashed line) and holes (stippled line) to the total drain current.

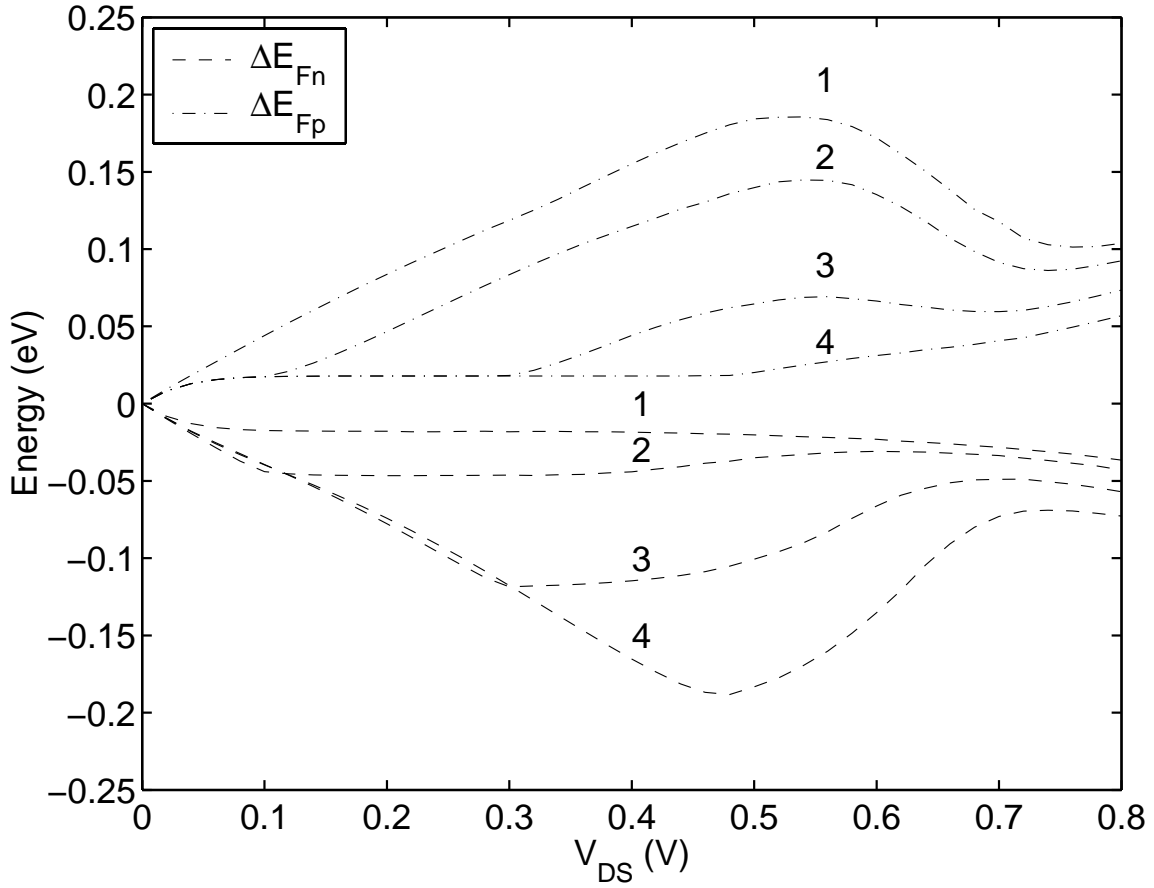


Figure 5: Dependence of QFL splits  $\Delta E_{Fn}$  and  $\Delta E_{Fp}$  on bias for: (1)  $V_{GS} = 0.0$  V, (2)  $V_{GS} = 0.1$  V, (3)  $V_{GS} = 0.3$  V, and (4)  $V_{GS} = 0.5$  V. Note that  $\Delta E_{Fn} = E_{Fn}$  and  $\Delta E_{Fp} = E_{Fp} + qV_{DS}$ , as shown in Figure 1, and  $E_{Fn}$  and  $E_{Fp}$  are negative values.

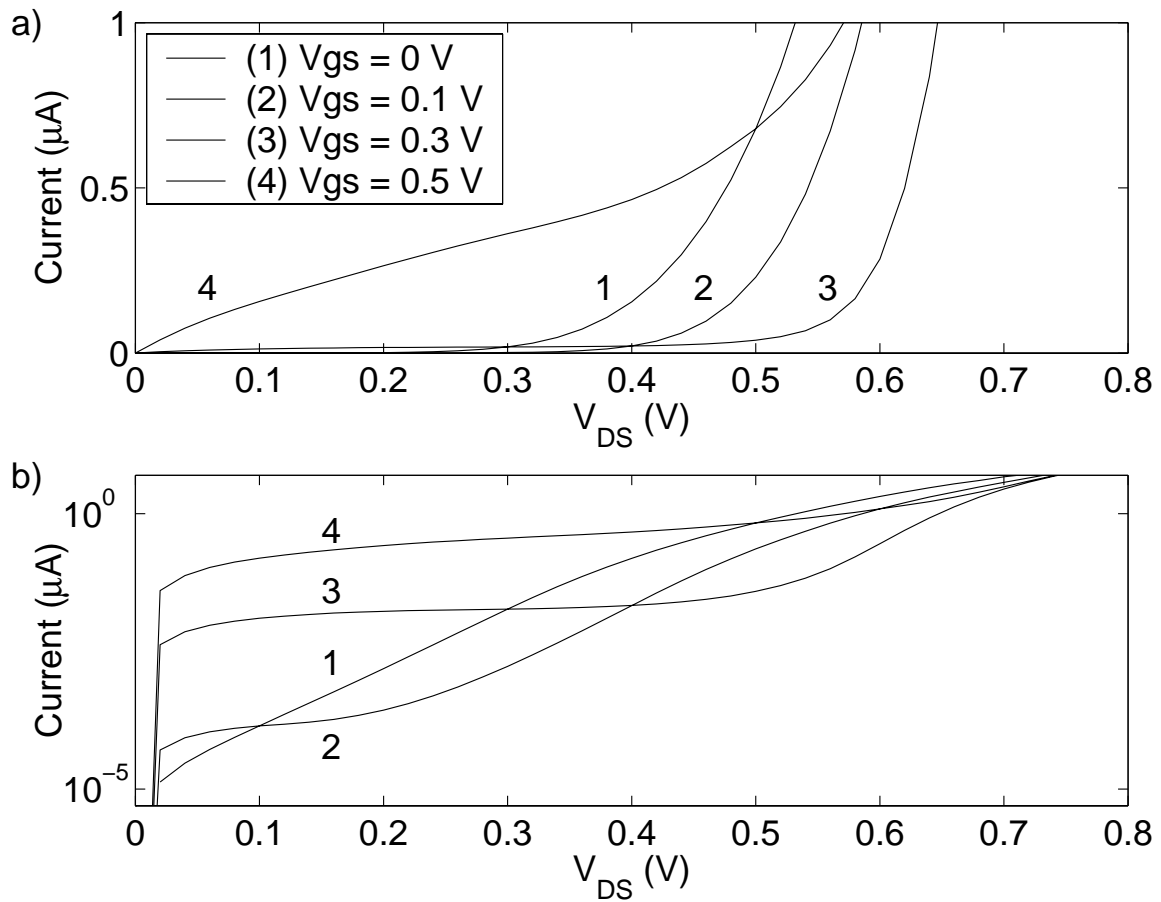


Figure 6: Drain  $I$ - $V$  characteristics: (a) linear plot, (b) log-linear plot.

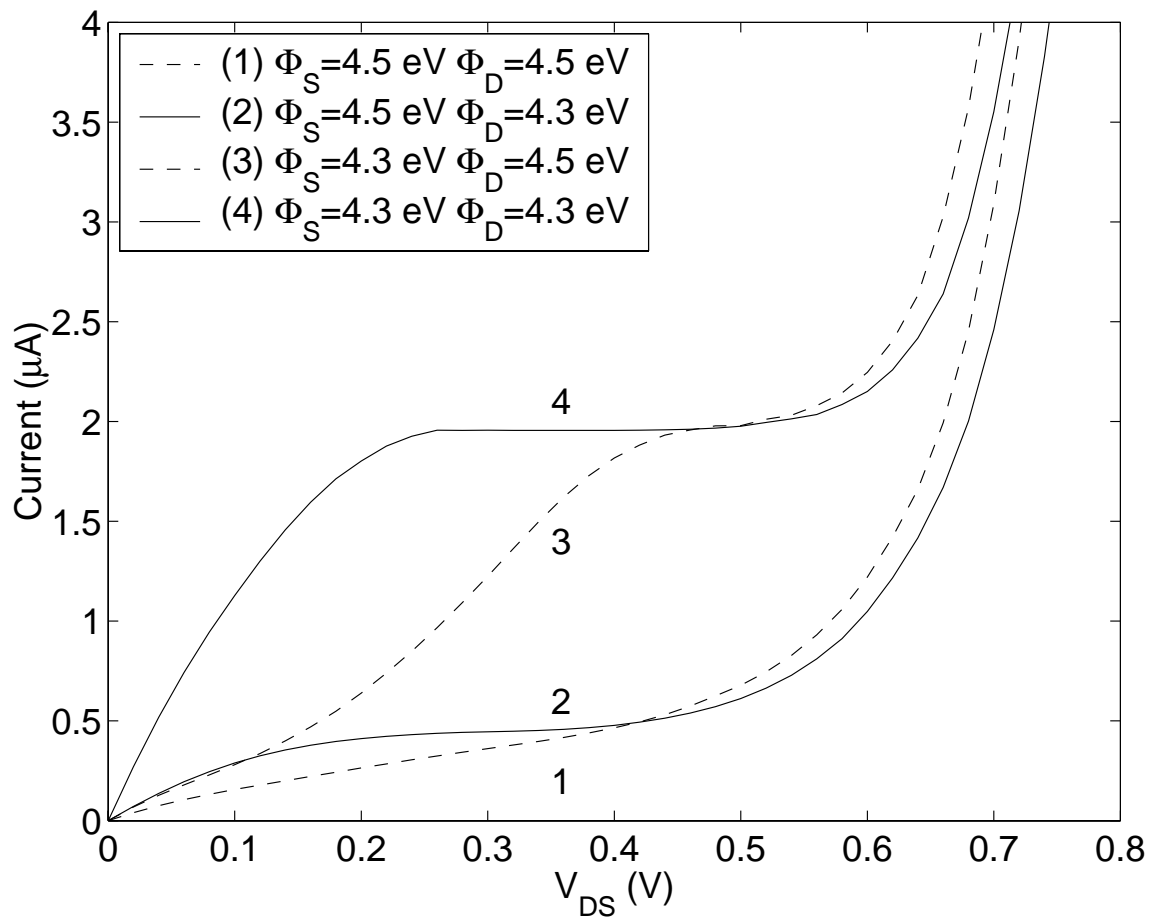


Figure 7: Drain  $I$ - $V$  characteristics for different workfunctions at the contacts to the nanotube at  $V_{GS} = 0.5 \text{ V}$ .